

Article

Design and Characterisation of a Fast Steering Mirror Compensation System Based on Double Porro Prisms by a Screw-Ray Tracing Method

Yu-Hao Chang ^{1,2}, Chien-Sheng Liu ^{1,3,*}  and Chih-Chun Cheng ^{1,2}

¹ Department of Mechanical Engineering, National Chung Cheng University, Chiayi County 62102, Taiwan; tako79716@gmail.com (Y.-H.C.); imeccc@ccu.edu.tw (C.-C.C.)

² Advanced Institute of Manufacturing with High-Tech Innovations, National Chung Cheng University, Chiayi County 62102, Taiwan

³ Department of Mechanical Engineering, National Cheng Kung University, Tainan City 70101, Taiwan

* Correspondence: cslu@mail.ncku.edu.tw; Tel.: +886-6-2757575 (ext. 62114)

Received: 19 October 2018; Accepted: 17 November 2018; Published: 20 November 2018



Abstract: This study proposes a novel FSM compensation system for four degrees of freedom (DOF) laser errors compensation, which has the advantage of shorter optical path length, fewer elements and an easier set-up process, meaning that it can be used at different locations. A commercial software, Zemax, is used to evaluate the function of the proposed FSM compensation system and the mathematical modelling of the proposed FSM compensation system is established by using a skew-ray tracing method. Finally, the proposed FSM compensation system is then verified experimentally using a laboratory-built prototype and the result shows that the proposed FSM compensation system achieves the ability to compensate the 4 DOF of the laser source.

Keywords: fast steer mirror; FSM; Double Porro prisms; laser drift; skew-ray tracing method

1. Introduction

Laser technology is widely utilised in different fields, such as engineering inspection, communication industry, semiconductor industry, and military industry [1–3]. Moreover, the stability of the laser device will directly influence the performance and the price of the equipment. However, the laser light is not a stable light source and it will ramble and shift as the time varies [4–7]. There are certain studies which mention that the intensity fluctuations of the laser source are related to the input current [8], while the environmental conditions (e.g., atmospheric), vibrations and thermally-induced motion may cause the laser to misalign [9]. The laser source drift contains two DOF angular errors and two DOF displacement errors, although even a small angular error will be magnified by the optical path length and reduce the quality of the product [10,11]. Therefore, it is necessary to improve the laser point stability. In order to solve the laser point stability problem, there are different types of methods which can be used to reduce the laser drift. The passive compensation method reduces the laser drift by controlling the power or frequency fluctuations of the laser device [12,13]. This method has a lower cost but also a lower efficiency; it cannot correct the laser point instantly and cannot correct the drift caused by environmental factors. By contrast, the fast steer mirror (FSM) compensation system can correct the laser point actively via its closed-loop system, and so it has the advantage of being able to correct the drift caused by environmental factors and the laser device itself; moreover, it can also compensate for the laser error instantly and continuously.

The FSM compensation system plays an important role in the free-space optical communications and auto adaptation optical system for controlling the laser beam direction, because it has good

dynamic performance [14–16]. In order to correct the 4 DOF laser errors to achieve the best laser point stability, there are two FSMs and two sensors which are used to correct the two angular errors and two displacement errors in the conventional FSM compensation system [17]. However, the conventional FSM compensation system has the disadvantage of longer optical path length, which means that errors are magnified due to the system's excessive elements. Therefore, this study proposes a new FSM compensation system that gives the existing compensation system the advantage of shorter optical path length, fewer elements, and easier set up at different locations. The proposed FSM compensation system is characterised using simulation methods and mathematical modelling, then evaluated by experimentally using a laboratory-built prototype.

2. Design of Proposed FSM Compensation System and Simulations

As shown in Figure 1, a conventional FSM compensation system is constructed using two 2-axes FSMs, two beam splitters, and two PSDs. In the FSM compensation system, PSDs play the role of detecting the four DOF laser source errors and the FSM is represented as a mirror that is mounted over the actuators to steer the output laser beam and compensate for laser errors. In order to achieve better laser point stability, it is necessary to compensate for all four DOF errors of the laser point. Therefore, the conventional FSM compensation system needs to place two 2-axes FSMs to compensate for the two DOF angular errors and the two DOF displacement errors respectively. However, these two 2-axes FSMs will produce an extra optical path between themselves, which means that the laser point will involve more environmental disturbance. Moreover, and as mentioned in Section 1, even a small angular error will be magnified by the optical path length, and thus it is essential to reduce the optical path length of the optical system.

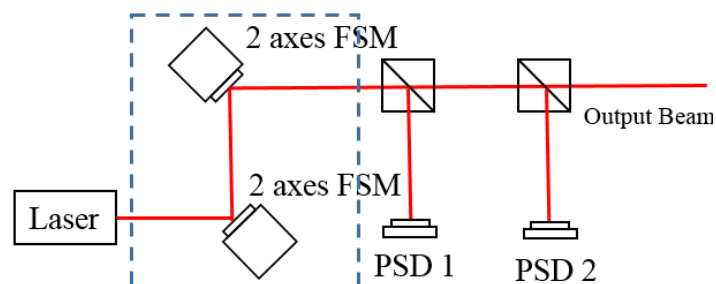


Figure 1. Optical path in conventional FSM compensation system.

This study proposes a new FSM structure to reduce the optical path length of the conventional FSM compensation system. As shown in Figure 2, the new FSM structure modifies the two FSMs to a new 4-axes FSM structure, which removes the optical path between two FSMs directly and reduces the environmental disturbance. However, one normal mirror could produce 2 DOF steering only, and so the Double Porro prisms, which could produce 4-DOF steering are used in the new FSM structure.

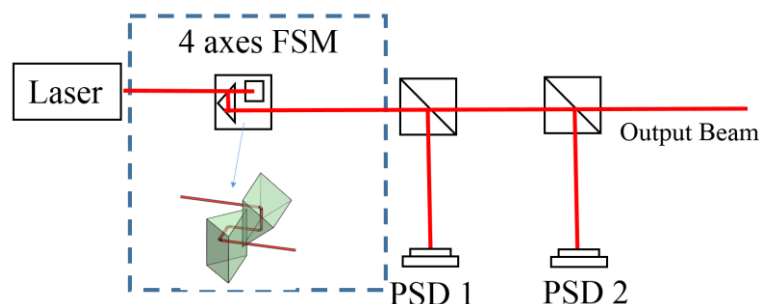


Figure 2. Optical path in proposed FSM compensation system.

Double Porro prisms are variants of the 90° prisms that are used as a pair to displace and invert a beam; indeed, these are widely employed in binoculars [18–20] and as a beam rotator [21]. As shown in Figure 3, the 90° prism could tilt and shift the laser path when the 90° prism is rotated along the Y-axis and shifted along the Y-axis; as such, when a pair of 90° prisms are put together vertically (which are called Double Porro prisms), they would have the ability of 4 DOF steering. Therefore, the characteristic of the Double Porro prisms mentioned above is combined with the 4-DOF actuator to compensate for the laser error.

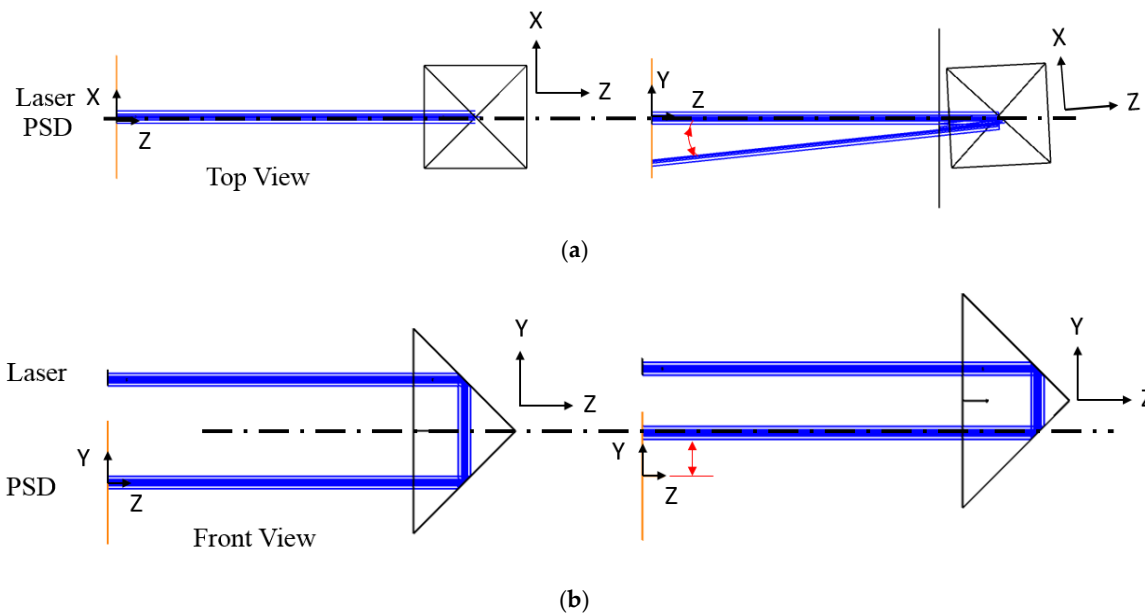


Figure 3. The schematic diagram of (a) the angular beam steering and (b) the translation beam steering of 90° prisms laser steering.

In order to verify the function of the proposed FSM compensation system, a commercial software, Zemax, is used to build the optical path and perform a multi-point laser error analysis which is shown in Figure 4. The analysis assigns the 2 DOF displacement errors and 2 DOF angular errors from -1 mm to $+1$ mm and from -1° to $+1^\circ$, respectively. Moreover, the distance and the angle between each interval are 0.1 mm and 0.1° , respectively. The distributions of 11^4 laser points are shown in Figure 5. However, all errors could be compensated for by the Double Porro prisms through the function of optimisation, which is shown in Figure 6; moreover, the compensated error is under 0.01 μm . The result verifies that the proposed FSM compensation system has the ability to compensate for 4 DOF laser errors and there is no singularity in the system.

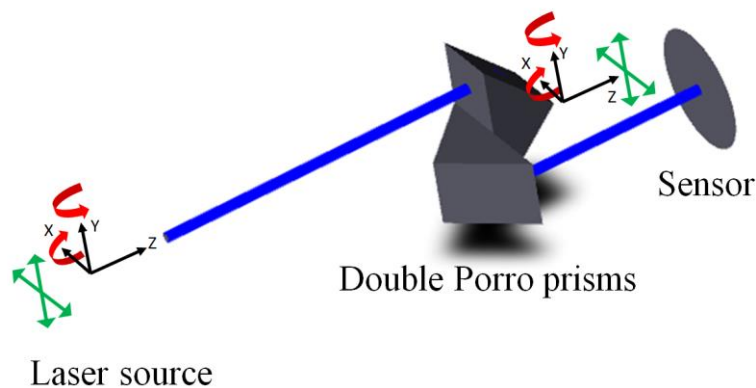


Figure 4. Compensation of four DOF laser errors in proposed FSM compensation system.

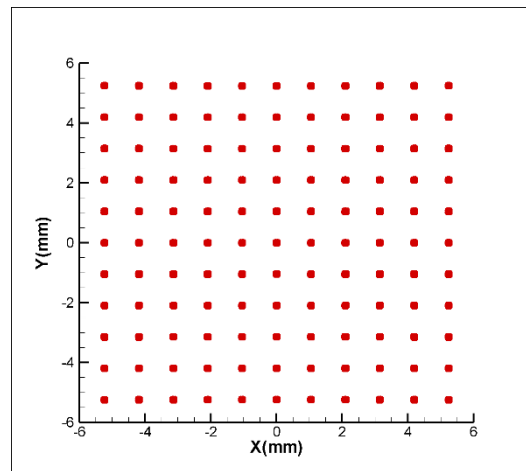


Figure 5. The distributions of laser points without compensation.

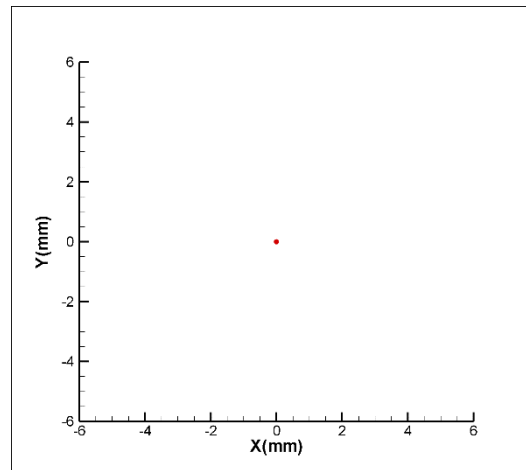


Figure 6. The distributions of laser points with compensation.

3. Proposed FSM Compensation Method

Firstly, the proposed FSM compensation system detects the laser drift by two PSDs and uses a mathematical algorithm to calculate the 2-DOF angular errors (θ_x, θ_y) and 2-DOF displacement errors (δ_x, δ_y), following which it calculates the compensation values ($\theta_x', \theta_y', \delta_x', \delta_y'$). Thereafter, the system drives the 4-axes actuator to compensate for the laser source errors.

3.1. Flat-Surface Skew-Ray Tracing Method

The flat-boundary skew-ray tracing method, proposed by Lin [18,22], is used in this study to build the mathematical algorithm of the proposed FSM compensation system. The transformation matrix ${}^R A_i$ is relative to the universal coordinate system (R) which is built on the boundary of each optical element, as shown below:

$${}^R A_i = \begin{bmatrix} I_{ix} & J_{ix} & K_{ix} & t_{ix} \\ I_{iy} & J_{iy} & K_{iy} & t_{iy} \\ I_{iz} & J_{iz} & K_{iz} & t_{iz} \\ 0 & 0 & 0 & 1 \end{bmatrix} \quad (1)$$

The vectors $\begin{bmatrix} I_{ix} & I_{iy} & I_{iz} & 0 \end{bmatrix}^T$, $\begin{bmatrix} J_{ix} & J_{iy} & J_{iz} & 0 \end{bmatrix}^T$ and $\begin{bmatrix} K_{ix} & K_{iy} & K_{iz} & 0 \end{bmatrix}^T$ describe the orientation of the three unit vectors of coordinate frame i with respect to another coordinate frame

R , respectively. Vector $\begin{bmatrix} t_{ix} & t_{iy} & t_{iz} & 0 \end{bmatrix}^T$ is the position vector of origin of coordinate frame i with respect to that of another coordinate frame R .

The laser ray is considered as unit direction vector in the flat-boundary skew-ray tracing method, as shown in Figure 7. P_{i-1} and ℓ_{i-1} express the incident point and incident unit direction vector, while P_i and ℓ_i express the point on the boundary and the reflected ray or refracted ray. They could be expressed as follows:

$$P_{i-1} = \begin{bmatrix} P_{i-1x} & P_{i-1y} & P_{i-1z} & 1 \end{bmatrix}^T \tag{2}$$

$$\ell_{i-1} = \begin{bmatrix} \ell_{i-1x} & \ell_{i-1y} & \ell_{i-1z} & 1 \end{bmatrix}^T \tag{3}$$

$$P_i = \begin{bmatrix} P_{ix} & P_{iy} & P_{iz} & 1 \end{bmatrix}^T = \begin{bmatrix} P_{i-1x} + \ell_{i-1x}\lambda_i & P_{i-1y} + \ell_{i-1y}\lambda_i & P_{i-1z} + \ell_{i-1z}\lambda_i & 1 \end{bmatrix}^T \tag{4}$$

λ_i is the geometrical length from the incident point P_{i-1} to the point on the boundary:

$$\lambda_i = \frac{-(I_{iz}P_{i-1x} + J_{iz}P_{i-1y} + K_{iz}P_{i-1z} + t_{iz})}{I_{iz}\ell_{i-1x} + J_{iz}\ell_{i-1y} + K_{iz}\ell_{i-1z}} = \frac{-B_i}{G_i} \tag{5}$$

According to Snell’s Law, when the laser incidents upon a flat surface and is reflected, the unit direction vector ℓ_i could be expressed as follows:

$$\ell_i = \begin{bmatrix} \ell_{ix} & \ell_{iy} & \ell_{iz} & 0 \end{bmatrix}^T = \begin{bmatrix} \ell_{i-1x} - 2I_{iz}G_i n_{ix} & \ell_{i-1y} - 2J_{iz}G_i n_{iy} & \ell_{i-1z} - 2K_{iz}G_i n_{iz} & 0 \end{bmatrix}^T \tag{6}$$

If the laser incident is refracted, the unit direction vector ℓ_i could be expressed as follows:

$$\ell_i = \begin{bmatrix} \ell_{ix} \\ \ell_{iy} \\ \ell_{iz} \\ 0 \end{bmatrix} = \begin{bmatrix} -n_{ix}\sqrt{1 - N_i^2 + (N_i C\theta_i)^2} + N_i(\ell_{i-1x} + n_{ix}C\theta_i) \\ -n_{iy}\sqrt{1 - N_i^2 + (N_i C\theta_i)^2} + N_i(\ell_{i-1y} + n_{iy}C\theta_i) \\ -n_{iz}\sqrt{1 - N_i^2 + (N_i C\theta_i)^2} + N_i(\ell_{i-1z} + n_{iz}C\theta_i) \\ 0 \end{bmatrix} \tag{7}$$

Note that n_i is normal vector and N_i is the index of refraction defined by Snell’s Law [23,24].

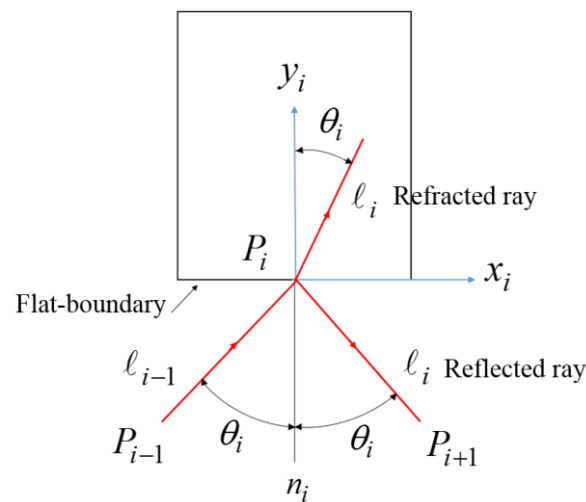


Figure 7. The schematic of refraction and reflection ray.

3.2. Laser Drift Errors Measurement

The proposed FSM compensation system includes two optical paths: the optical path I, which is from the laser source to PSD 1, and the optical path II to PSD 2, as shown in Figure 8. In order to

build the full skew-ray tracing of the proposed FSM compensation system, in the beginning coordinate system, the homogeneous coordinate transformation matrix of each boundary, incident point, and incident unit direction vector should be defined. As shown, the reference coordinate system $(xyz)_0$ is built on the laser source, while the coordinate $(xyz)_i$ is built on the boundary of optical elements; moreover, the parameters of the homogeneous coordinate transformation matrix of the coordinate system $(xyz)_i$ relative to $(xyz)_{i+1}$ are shown in Table 1. L_i is the straight-line distance between each coordinate system.

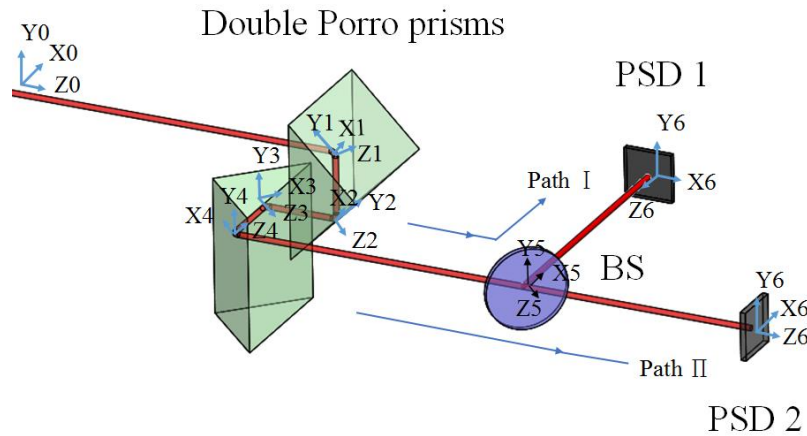


Figure 8. Spatial geometric configuration for Laser drift errors measurement.

Table 1. Coordinate transformation matrix parameters of laser drift errors measurement.

<i>i</i>	<i>i</i> = 1	<i>i</i> = 2	<i>i</i> = 3	<i>i</i> = 4	<i>i</i> = 5	<i>i</i> = 6	<i>i</i> = 6
Optical Element	Double Porro Prisms	Double Porro Prisms	Double Porro Prisms	Double Porro Prisms	BS	PSD 1	PSD 2
I_{ix}	1	1	$1/\sqrt{2}$	0	$1/\sqrt{2}$	$1/\sqrt{2}$	$1/\sqrt{2}$
I_{iy}	0	0	0	0	0	0	0
I_{iz}	0	0	$-1/\sqrt{2}$	1	$-1/\sqrt{2}$	$-1/\sqrt{2}$	$1/\sqrt{2}$
J_{ix}	0	0	1/2	0	0	0	0
J_{iy}	$1/\sqrt{2}$	0	$1/\sqrt{2}$	1	1	1	1
J_{iz}	$1/\sqrt{2}$	-1	1/2	0	0	0	0
K_{ix}	0	0	1/2	-1	$1/\sqrt{2}$	$1/\sqrt{2}$	$1/\sqrt{2}$
K_{iy}	$-1/\sqrt{2}$	1	$-1/\sqrt{2}$	0	0	0	0
K_{iz}	$1/\sqrt{2}$	0	1/2	0	$1/\sqrt{2}$	$1/\sqrt{2}$	$1/\sqrt{2}$
t_{ix}	$L2_x$	$L3_x$	$L4_x$	$L5_x$	$L7_x$	$L8_x$	$L8_x$
t_{iy}	$L2_y$	$L3_y$	$L4_y$	$L5_y$	$L7_y$	$L8_y$	$L8_y$
t_{iz}	$L2_z$	$L3_z$	$L4_z$	$L5_z$	$L7_z$	$L8_z$	$L8_z$

The incident point and incident unit direct vector of the laser source relative to the reference coordinate system are defined as:

$$P_0 = [0 \ 0 \ 0 \ 1]^T, \ell_0 = [0 \ 0 \ 1 \ 0]^T \tag{8}$$

A transformation matrix T_1 is used to distinguish between 2-DOF angular errors (θ_x, θ_y) and 2-DOF displacement errors (δ_x, δ_y) of laser drift:

$$T_1 = \begin{bmatrix} 1 & 0 & 0 & \delta_x \\ 0 & 1 & 0 & \delta_y \\ 0 & 0 & 1 & 0 \\ 0 & 0 & 0 & 1 \end{bmatrix} \begin{bmatrix} 1 & 0 & 0 & 0 \\ 0 & \cos(\theta_x) & -\sin(\theta_x) & 0 \\ 0 & \sin(\theta_x) & \cos(\theta_x) & 0 \\ 0 & 0 & 0 & 1 \end{bmatrix} \begin{bmatrix} \cos(\theta_y) & 0 & \sin(\theta_y) & 0 \\ 0 & 1 & 0 & 0 \\ -\sin(\theta_y) & 0 & \cos(\theta_y) & 0 \\ 0 & 0 & 0 & 0 \end{bmatrix} \tag{9}$$

Furthermore, the laser source containing 2-DOF angular errors (θ_x, θ_y) and 2-DOF displacement error (δ_x, δ_y) could be written as:

$$P_0' = T_1 P_0, \ell_0' = T_1 \ell_0 \tag{10}$$

The laser ray on the coordinate $(xyz)_0$ would incident to the first optical boundary $(xyz)_1$, then reflect to the next optical boundary $(xyz)_2$. The incident point 1P_1 and the reflected ray ${}^1\ell_1$ on the first optical boundary, which are relative to coordinate $(xyz)_1$, could be calculated by using Equation (4) to Equation (6) and the parameter of the homogeneous coordinate transformation matrix 1A_0 of the coordinate system $(xyz)_0$ relative to $(xyz)_1$, as shown in Table 1. Now the 1P_1 and ${}^1\ell_1$ are considered as the incident point and the incident unit direct vector of the next optical boundary $(xyz)_2$; as such, the same method mentioned above is then used to obtain the incident points 2P_2 and ${}^2\ell_2$ on the second optical boundary, which are relative to coordinate $(xyz)_2$. Sequentially, the incident point and the incident unit direct vector on each optical boundary could be obtained. Finally, the spot coordinates on PSD 1 and PSD 2 could be obtained as simultaneous higher order equations in four variables as follows:

$$P_{PSD1} = \begin{bmatrix} X_1(\theta_x, \theta_y, \delta_x, \delta_y) & Y_1(\theta_x, \theta_y, \delta_x, \delta_y) & 0 & 1 \end{bmatrix} \tag{11}$$

$$P_{PSD2} = \begin{bmatrix} X_2(\theta_x, \theta_y, \delta_x, \delta_y) & Y_2(\theta_x, \theta_y, \delta_x, \delta_y) & 0 & 1 \end{bmatrix} \tag{12}$$

After the whole flat-boundary skew-ray tracing, the relationship between PSD 1, PSD 2, and the four laser drift errors is built as Equations (11) and (12), where, X_1, X_2, Y_1 and Y_2 are the coordinate values of X and Y direction on PSD 1 and PSD 2, respectively. The four laser drift errors could be obtained after solving Equations (11) and (12):

$$\theta_x = f_1(X_1, X_2, Y_1, Y_2) \tag{13}$$

$$\theta_y = f_2(X_1, X_2, Y_1, Y_2) \tag{14}$$

$$\delta_x = f_3(X_1, X_2, Y_1, Y_2) \tag{15}$$

$$\delta_y = f_4(X_1, X_2, Y_1, Y_2) \tag{16}$$

3.3. Laser Drift Errors Compensation

This section builds a new coordinate system to calculate the compensation values of the Double Porro prisms, which is shown in Figure 9. The parameters of the homogeneous coordinate transformation matrix of the coordinate system $(xyz)_i$ relative to $(xyz)_{i+1}$ are shown in Table 2.

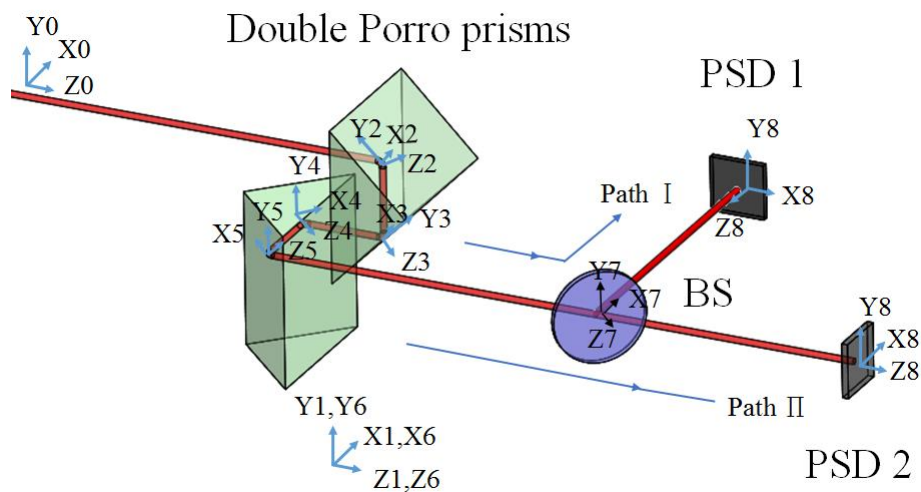


Figure 9. Spatial geometric configuration for Laser drift errors compensation.

Table 2. Coordinate transformation matrix parameters of laser drift errors compensation.

i	$i = 1$	$i = 2$	$i = 3$	$i = 4$	$i = 5$	$i = 6$	$i = 7$	$i = 8$	$i = 8$
Optical Element	4-Axes Actuator	Double Porro Prisms	Double Porro Prisms	Double Porro Prisms	Double Porro Prisms	4-Axes Actuator	BS	PSD 1	PSD 2
N_i	1	reflected	reflected	reflected	reflected	1	reflected		
I_{ix}	1	1	1	$1/\sqrt{2}$	0	$1/\sqrt{2}$	$1/\sqrt{2}$	$1/\sqrt{2}$	$1/\sqrt{2}$
I_{iy}	0	0	0	0	0	0	0	0	0
I_{iz}	0	0	0	$-1/\sqrt{2}$	1	$-1/\sqrt{2}$	$-1/\sqrt{2}$	$-1/\sqrt{2}$	$1/\sqrt{2}$
J_{ix}	0	0	0	$1/2$	0	0	0	0	0
J_{iy}	1	$1/\sqrt{2}$	0	$1/\sqrt{2}$	1	1	1	1	1
J_{iz}	0	$1/\sqrt{2}$	-1	$1/2$	0	0	0	0	0
K_{ix}	0	0	0	$1/2$	-1	$1/\sqrt{2}$	$1/\sqrt{2}$	$1/\sqrt{2}$	$1/\sqrt{2}$
K_{iy}	0	$-1/\sqrt{2}$	1	$-1/\sqrt{2}$	0	0	0	0	0
K_{iz}	1	$1/\sqrt{2}$	0	$1/2$	0	$1/\sqrt{2}$	$1/\sqrt{2}$	$1/\sqrt{2}$	$1/\sqrt{2}$
t_{ix}	$L1_x$	$L2_x$	$L3_x$	$L4_x$	$L5_x$	$L6_x$	$L7_x$	$L8_x$	$L8_x$
t_{iy}	$L1_y$	$L2_y$	$L3_y$	$L4_y$	$L5_y$	$L6_y$	$L7_y$	$L8_y$	$L8_y$
t_{iz}	$L1_z$	$L2_z$	$L3_z$	$L4_z$	$L5_z$	$L6_z$	$L7_z$	$L8_z$	$L8_z$

The coordinate system $(xyz)_1$ and $(xyz)_6$ are set under the Double Porro prisms, which simulate the motion of the 4-axes actuator. The incident point and incident unit direct vector of a laser source that contains 4-DOF errors could be written as:

$$P_0' = T_1 P_0, \ell_0' = T_1 \ell_0 \quad (17)$$

Note that the angular errors (θ_x, θ_y) and displacement errors (δ_x, δ_y) are known to be constant in this sub-section. The laser ray on the coordinate $(xyz)_0$ would incident to the first virtual boundary $(xyz)_1$, then refract to the next optical boundary $(xyz)_2$. The transformation matrices T_2 and T_3 are used to describe 2-DOF angular motion (θ_x', θ_y') and 2-DOF displacement motion (δ_x', δ_y') of Double Porro prisms:

$$T_2 = \begin{bmatrix} 1 & 0 & 0 & \delta_x' \\ 0 & 1 & 0 & \delta_y' \\ 0 & 0 & 1 & 0 \\ 0 & 0 & 0 & 1 \end{bmatrix} \begin{bmatrix} 1 & 0 & 0 & 0 \\ 0 & \cos(\theta_x') & -\sin(\theta_x') & 0 \\ 0 & \sin(\theta_x') & \cos(\theta_x') & 0 \\ 0 & 0 & 0 & 1 \end{bmatrix} \begin{bmatrix} \cos(\theta_y') & 0 & \sin(\theta_y') & 0 \\ 0 & 1 & 0 & 0 \\ -\sin(\theta_y') & 0 & \cos(\theta_y') & 0 \\ 0 & 0 & 0 & 0 \end{bmatrix} \quad (18)$$

$$T_3 = \begin{bmatrix} 1 & 0 & 0 & -\delta_x' \\ 0 & 1 & 0 & -\delta_y' \\ 0 & 0 & 1 & 0 \\ 0 & 0 & 0 & 1 \end{bmatrix} \begin{bmatrix} 1 & 0 & 0 & 0 \\ 0 & \cos(-\theta_x') & -\sin(-\theta_x') & 0 \\ 0 & \sin(-\theta_x') & \cos(-\theta_x') & 0 \\ 0 & 0 & 0 & 1 \end{bmatrix} \begin{bmatrix} \cos(-\theta_y') & 0 & \sin(-\theta_y') & 0 \\ 0 & 1 & 0 & 0 \\ -\sin(-\theta_y') & 0 & \cos(-\theta_y') & 0 \\ 0 & 0 & 0 & 0 \end{bmatrix}$$

Of particular note here are the homogeneous coordinate transformation matrix ${}^0A_1'$ of the coordinate system $(xyz)_1$ relative to $(xyz)_0$ and ${}^5A_6'$ of the coordinate system $(xyz)_5$ relative to $(xyz)_6$, which contain 4-DOF variables to transfer the boundary of Double Porro prisms. These are expressed as follows:

$${}^1A_0' = T_2 {}^1A_0 \quad (19)$$

$${}^6A_5' = T_2 {}^6A_5 \quad (20)$$

The incident point 1P_1 and the refracted ray ${}^1\ell_1$ on the first virtual boundary, which are relative to coordinate $(xyz)_1$, could be calculated by using Equation (4) to Equations (6), (7) and (19). The same method mentioned in the last section is used sequentially to obtain the incident point and incident unit direct vector on each optical boundary. Finally, the spot coordinates on PSD 1 and PSD 2 could be obtained as simultaneous higher order equations in four variables as follows:

$$P_{PSD1} = \begin{bmatrix} X_1(\theta_x', \theta_y', \delta_x', \delta_y') & Y_1(\theta_x', \theta_y', \delta_x', \delta_y') & 0 & 1 \end{bmatrix} \quad (21)$$

$$P_{PSD2} = \begin{bmatrix} X_2(\theta_x', \theta_y', \delta_x', \delta_y') & Y_2(\theta_x', \theta_y', \delta_x', \delta_y') & 0 & 1 \end{bmatrix} \quad (22)$$

The relationship between PSD 1, PSD 2 and 4-DOF motion of Double Porro prisms is built as Equations (21) and (22), where, X_1 , X_2 , Y_1 and Y_2 are the coordinate values of X and Y direction on PSD 1 and PSD 2, respectively. Consequently, the four laser drift errors could be obtained after solving Equations (21) and (22):

$$\theta_x' = f_1(X_1, X_2, Y_1, Y_2) \quad (23)$$

$$\theta_y' = f_2(X_1, X_2, Y_1, Y_2) \quad (24)$$

$$\delta_x' = f_3(X_1, X_2, Y_1, Y_2) \quad (25)$$

$$\delta_y' = f_4(X_1, X_2, Y_1, Y_2) \quad (26)$$

4. Experimental Setup and Results

The prototype of the proposed FSM compensation system is set on the optical bench as shown in Figure 10. As can be seen, this experiment involves the use of a He-Ne laser (EL01A, 632 nm, 10 mW, LASOS, Jena, Germany), a 2-axis linear translation stage, a 2-axis rotation stage, a “Stewart Platform” type hexapod (HXP50-MECA, Newport, Irvine, CA, USA), a double Porro prisms composed of two hollow-roof prism mirrors, a beam splitter and two dual-axis lateral PSDs (SPOTANA-9S-USB-L, DUMA OPTRONICS, Neshar, Israel). A He-Ne laser is used as the light source, which is firstly set on the 2-axis linear translation stage.

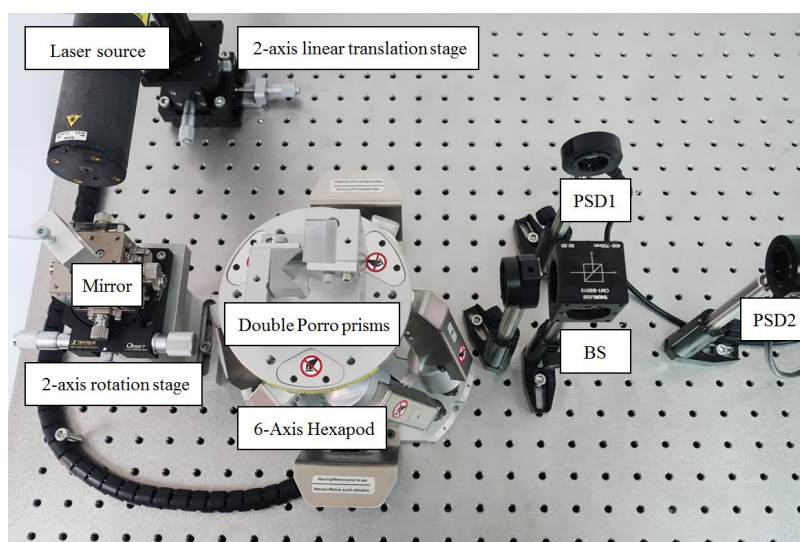


Figure 10. Photograph of experimental setup.

Following this, the laser source incidents to a mirror which is set on the 2-axis rotation stage and then reflects to the Double Porro prisms which are set on a 6-axis hexapod. The laser beam is then directed into a beam splitter (BS). Finally, the laser beam is split into PSD 1 and PSD 2 by the BS. The 2-axis linear translation stage and 2-axis rotation stage are applied to produce 4-DOF laser errors, namely θ_x , θ_y , δ_x and δ_y , at the same time. The 6-axis Hexapod is a parallel kinematic motion device that provides 6-DOF motion, which is applied to produce 4-DOF motion θ_x' , θ_y' , δ_x' and δ_y' to compensate for the laser errors. The progress of the experiment is as follows. In the beginning, 4 DOF laser errors, θ_x , θ_y , δ_x and δ_y , are produced by the linear translation stage separately, following which PSD 1 and PSD 2 detect the signals of the laser spots. Moreover, a commercial software, MATLAB, is used to solve the laser errors and the compensation values through the reading of two PSDs. Lastly, the Double Porro prisms are driven to compensate for the 4 DOF laser errors.

Figure 11a,b show the experimental results for the variation of positions of light spots on the PSDs with and without the compensation, when the laser error is $\delta_x = 50$ and $\delta_x = -50$ μm , respectively. As shown in Figure 11a, the readings of PSD1 and PSD are -50 and 50 μm when $\delta_x = 50$ μm . After

compensating for the laser error, the readings of PSD 1 and PSD 2 are reduced to approximately $0 \mu\text{m}$, which means that the laser error of $\delta_x = 50 \mu\text{m}$ is compensated for by the proposed FSM compensation system. The same is seen in Figure 11b, where the result shows that the readings of two PSDs are reduced to around $0 \mu\text{m}$, which means that the laser error of $\delta_x = -50 \mu\text{m}$ is compensated for by the proposed FSM compensation system. Figure 12a,b show the experimental results for the variation of positions of light spots on the PSDs with and without the compensation, when the laser error is $\delta_y = 50$ and $\delta_y = -50 \mu\text{m}$, respectively. As shown, both the laser errors of $\delta_y = 50$ and $\delta_y = -50 \mu\text{m}$ are compensated for by the proposed FSM compensation system. Figure 13a,b show the experimental results for the variation of positions of light spots on the PSDs with and without the compensation, when the laser error is $\theta_x = 0.1$ and $\theta_x = -0.1^\circ$, respectively. As shown, both the laser errors of $\theta_x = 0.1$ and $\theta_x = -0.1$ degrees are compensated for by the proposed FSM compensation system. Figure 14a,b show the experimental results for the variation of positions of light spots on the PSDs with and without the compensation, when the laser error is $\theta_y = 0.1$ and $\theta_y = -0.1^\circ$, respectively. As shown, both the laser errors of $\theta_y = 0.1$ and $\theta_y = -0.1^\circ$ are compensated for by the proposed FSM compensation system. Figure 15 shows the experimental results for the variation of positions of light spots on the PSDs with and without the compensation when the laser error has 4 DOF errors of $\theta_x = -0.1^\circ$, $\theta_y = -0.1^\circ$, $\delta_x = -50 \mu\text{m}$ and $\delta_y = -50 \mu\text{m}$. As shown, 4 DOF laser errors are compensated for by the proposed FSM compensation system. It demonstrates the feasibility of the proposed FSM compensation system.

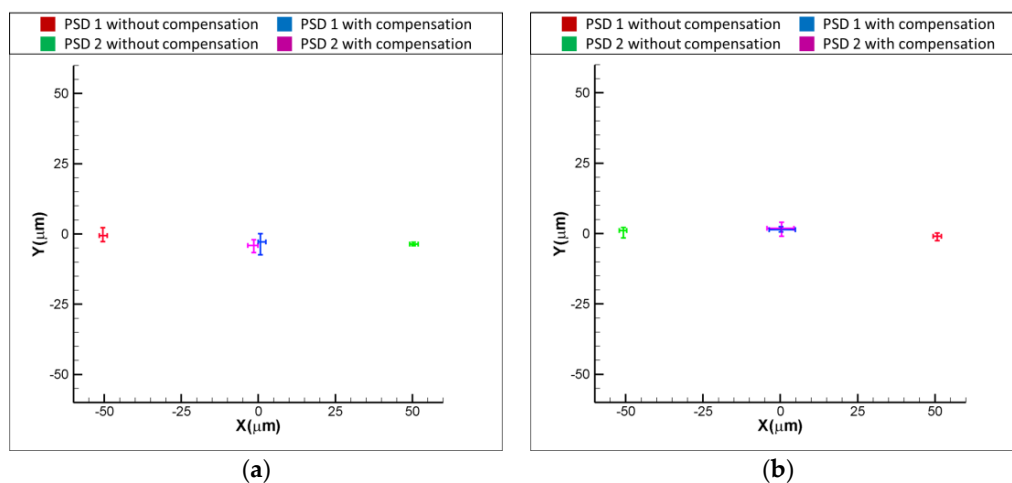


Figure 11. Experimental results for variation of positions of light spots on PSDs with and without compensation (a) $\delta_x = 50$ and (b) $\delta_x = -50 \mu\text{m}$, respectively.

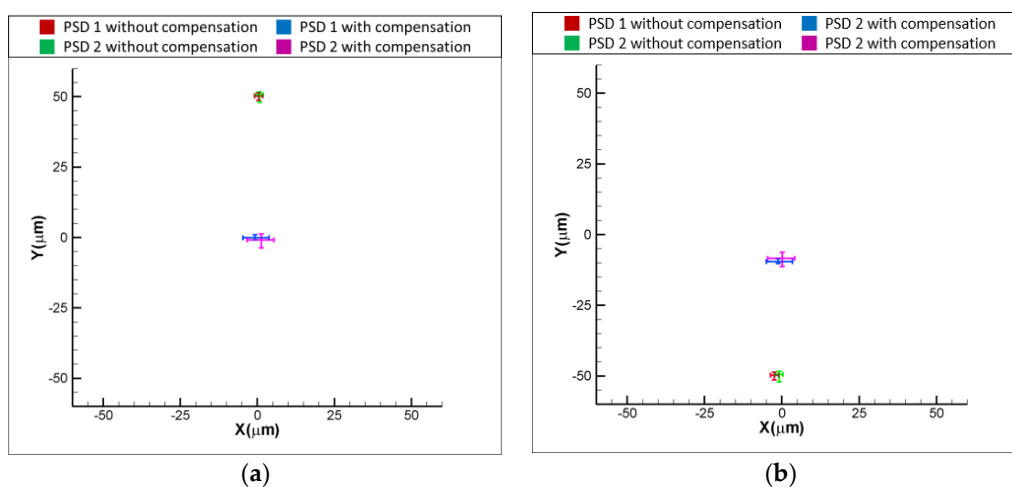


Figure 12. Experimental results for variation of positions of light spots on PSDs with and without compensation (a) $\delta_y = 50$ and (b) $\delta_y = -50 \mu\text{m}$, respectively.

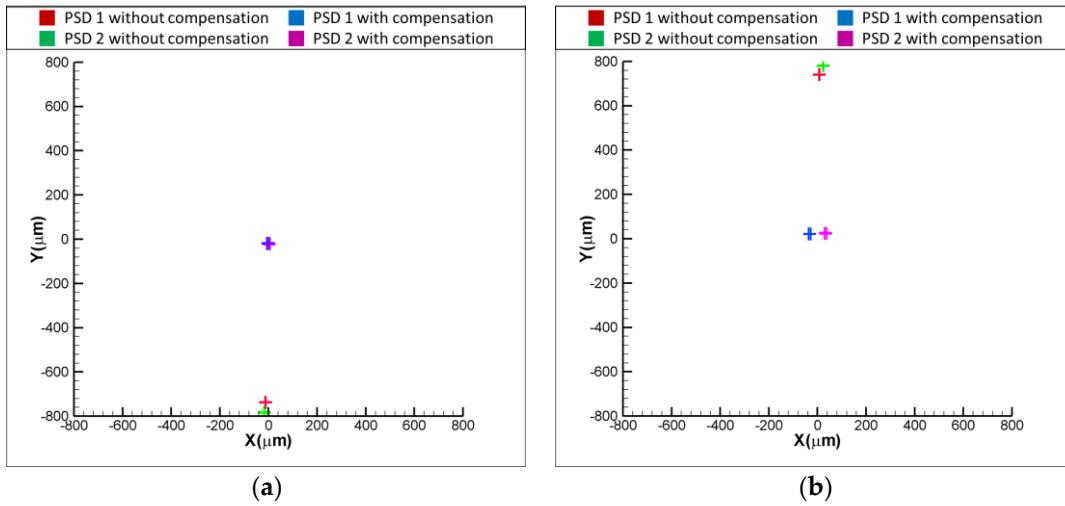


Figure 13. Experimental results for variation of positions of light spots on PSDs with and without compensation (a) $\theta_x = 0.1$ and (b) $\theta_x = -0.1^\circ$, respectively.

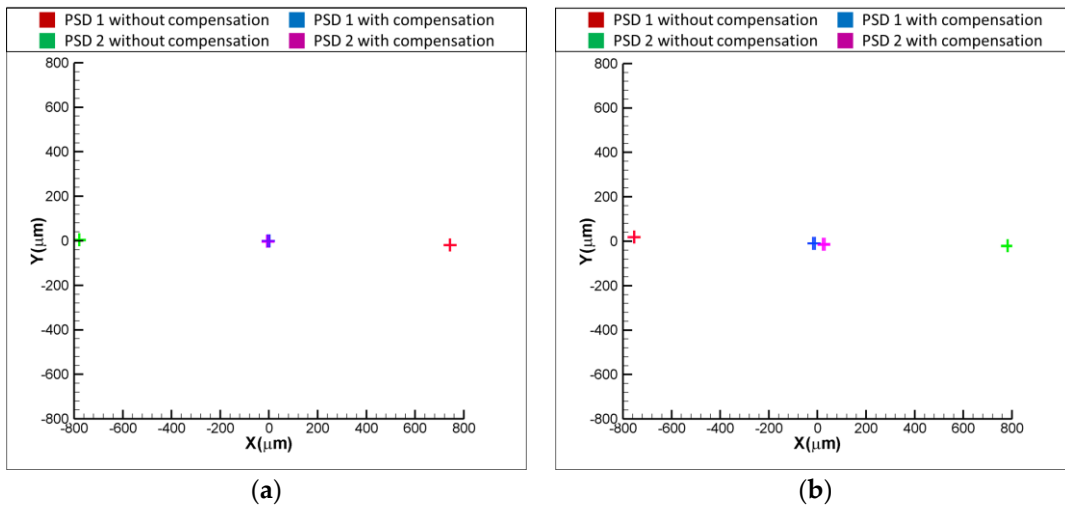


Figure 14. Experimental results for variation of positions of light spots on PSDs with and without compensation (a) $\theta_y = 0.1$ and (b) $\theta_y = -0.1^\circ$, respectively.

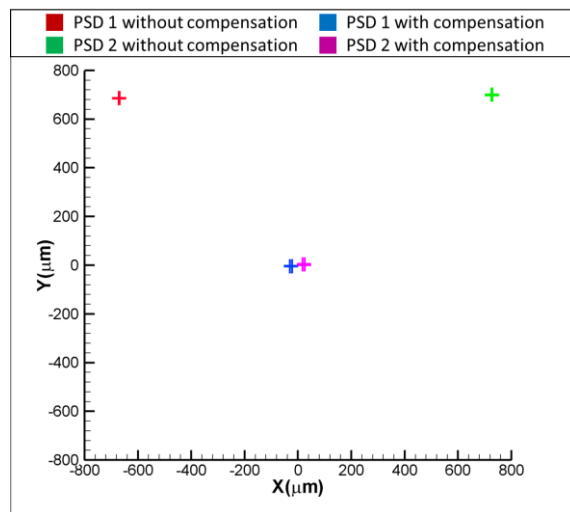


Figure 15. Experimental results for variation of positions of light spots on PSDs with and without compensation when $\theta_x = -0.1^\circ$, $\theta_y = -0.1^\circ$, $\delta_x = -50 \mu\text{m}$ and $\delta_y = -50 \mu\text{m}$.

5. Error Analysis

The mathematical modelling of the proposed FSM compensation system is established by using a skew-ray tracing method. However, the real optics system is not exactly the same as the mathematical model due to installation errors of each optical element. The installation errors affect the reading of the PSD and reduce the optical accuracy directly. Therefore, it is essential to analyse the influence of each installation error for the optical elements.

For the purpose of installation error analysis, each optical element is provided with 6 DOF installation errors respectively in order to observe the influence of installation error on the FSM compensation system; moreover, the coordinate system is shown in Figure 9. Figures 16–19 show the installation error analysis of double Porro prisms, BS, PSD 1 and PSD 2 when laser errors are $\delta_x = 1$ mm, $\delta_y = 1$ mm, $\theta_x = -1^\circ$ and $\theta_y = -1^\circ$.

The translational installation errors ($'\delta_x$, $'\delta_y$ and $'\delta_z$) and the rotational installation errors ($'\theta_x$, $'\theta_y$ and $'\theta_z$) are defined as -0.5 mm to 0.5 mm and -0.5° to 0.5° . As shown in Figures 16–19, the installation errors of $'\delta_z$, $'\theta_x$, $'\theta_y$ and $'\theta_z$ of each optical element affect the accuracy of the laser error measurement, but $'\delta_x$ and $'\delta_y$ do not. Furthermore, the result of installation error analysis shows that the installation error $'\theta_z$ of PSD 2 is critical in the FSM compensation system due to the fact that it has the longest optical length.

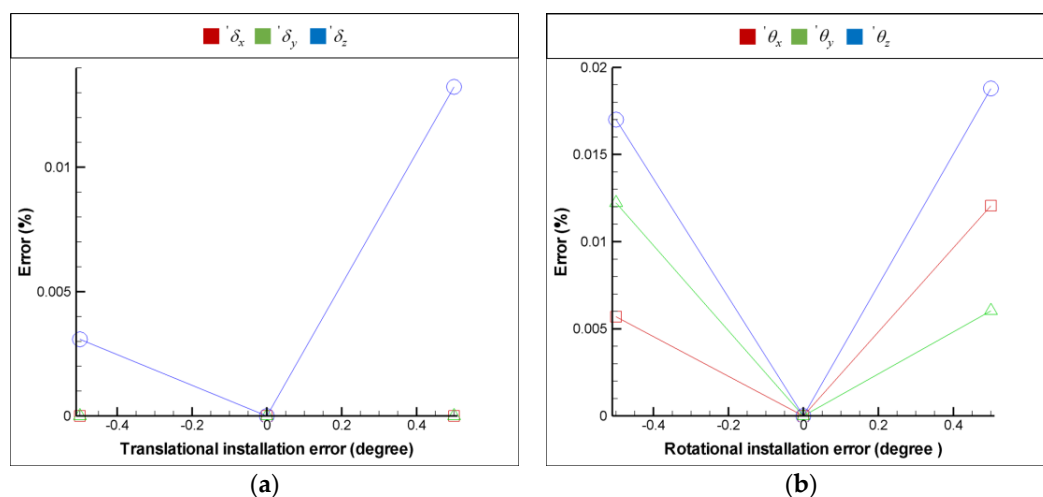


Figure 16. Installation error analysis of double Porro prisms for (a) translational installation errors ($'\delta_x$, $'\delta_y$ and $'\delta_z$) and (b) translational installation errors ($'\theta_x$, $'\theta_y$ and $'\theta_z$).

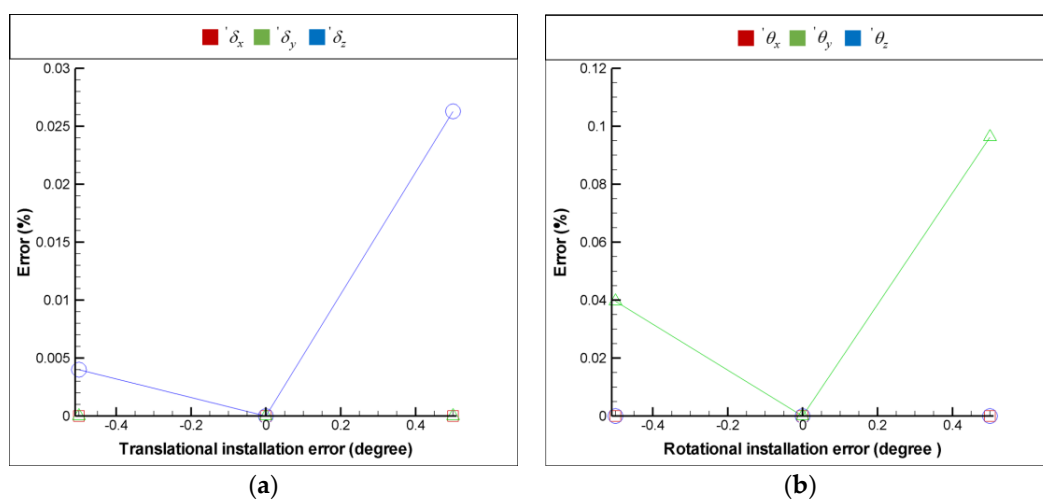


Figure 17. Installation error analysis of double BS for (a) translational installation errors ($'\delta_x$, $'\delta_y$ and $'\delta_z$) and (b) translational installation errors ($'\theta_x$, $'\theta_y$ and $'\theta_z$).

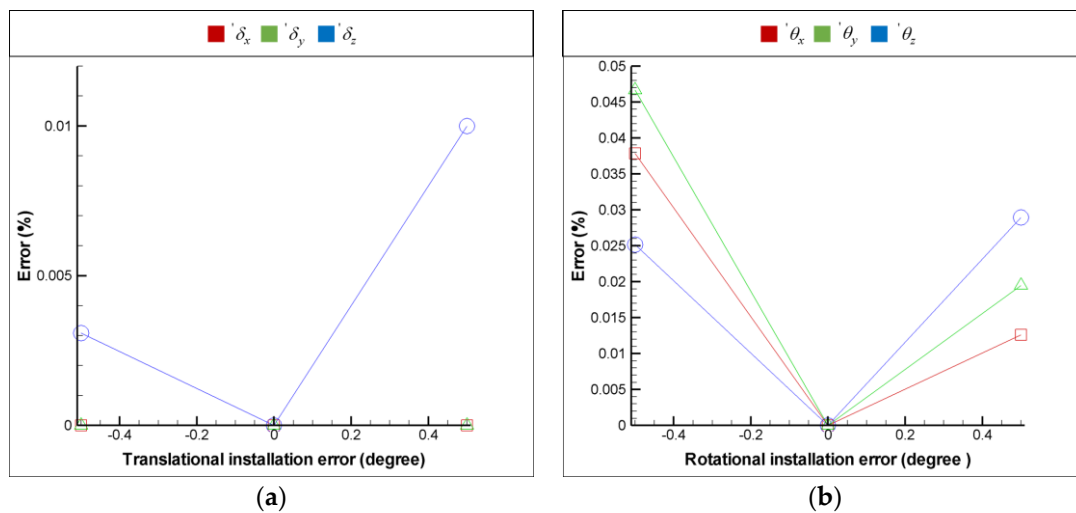


Figure 18. Installation error analysis of double PSD 1 for (a) translational installation errors (δ_x , δ_y and δ_z) and (b) translational installation errors (θ_x , θ_y and θ_z).

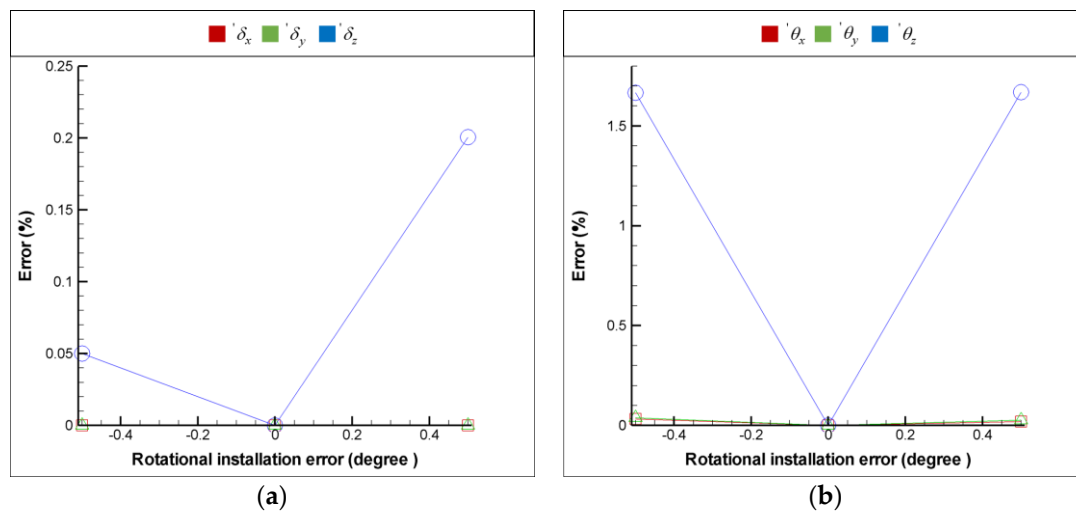


Figure 19. Installation error analysis of double PSD 2 for (a) translational installation errors (δ_x , δ_y and δ_z) and (b) translational installation errors (θ_x , θ_y and θ_z).

6. Conclusions

This study has presented a new FSM compensation system with Double Porro prisms to compensate for the 4 DOF laser errors of the laser source, which is characterised by shorter optical path length, fewer elements and easier set up at different locations. The performance of the proposed FSM compensation system has been evaluated using a laboratory-built prototype. The experiment results show that the proposed FSM compensation system can eliminate 97% of the laser errors. This implies that the proposed FSM compensation system has the ability to measure and compensate for laser errors.

7. Patents

The authors have not published any patent from the work reported in this manuscript.

Author Contributions: Conceptualisation, Y.-H.C.; methodology, Y.-H.C.; validation, Y.-H.C.; writing—original draft preparation, Y.-H.C.; writing—review and editing, Y.-H.C., C.-S.L. and C.-C.C.; supervision, project administration, and funding acquisition, C.-S.L. and C.-C.C.

Funding: This research was funded by the Ministry of Science and Technology of Taiwan, grant numbers MOST 105-2221-E-006-265-MY5 and 106-2628-E-006-010-MY3.

Conflicts of Interest: The authors declare no conflict of interest.

Abbreviations

θ_x	The laser angular error which rotates along the x axis.
θ_y	The laser angular error which rotates along the y axis.
δ_x	The laser displacement error which translates along the x axis.
δ_y	The laser displacement error which translates along the y axis.
θ'_x	The angular motion of Porro prisms which rotate along the x axis.
θ'_y	The angular motion of Porro prisms which rotate along the y axis.
δ'_x	The displacement motion of Porro prisms which translate along the x axis.
δ'_y	The displacement motion of Porro prisms which translate along the y axis.
${}^R A_i$	The pose matrix i with respect to coordinate system R .
I	The unit vector of the coordinate system i on the x direction with respect to the coordinate system R .
J	The unit vector of the coordinate system i on the y direction with respect to the coordinate system R .
K	The unit vector of the coordinate system i on the z direction with respect to the coordinate system R .
t	The position vector of the origin of the coordinate system i with respect to the coordinate system R .
P_{i-1}	The incident point of light source.
P_i	The incident point at the i th optic boundary.
ℓ_{i-1}	The incident unit direction vector of a light source at point P_{i-1} .
ℓ_i	The unit directional vector of a light ray after being reflected or refracted by optic boundary.
$'\theta_x$	The installation error which rotates along the x axis.
$'\theta_y$	The installation error which rotates along the y axis.
$'\theta_z$	The installation error which rotates along the z axis.
$'\delta_x$	The installation error which translates along the x axis.
$'\delta_y$	The installation error which translates along the y axis.
$'\delta_z$	The installation error which translates along the z axis.

References

- Dong, Z.; Sun, X.; Liu, W.; Yang, H. Measurement of free-form curved surfaces using laser triangulation. *Sensors* **2018**, *18*, 3527. [[CrossRef](#)] [[PubMed](#)]
- Duan, L.; Zhang, H.; Shi, W.; Yang, X.; Lu, Y.; Yao, J. High-resolution temperature sensor based on single-frequency ring fiber laser via optical heterodyne spectroscopy technology. *Sensors* **2018**, *18*, 3245. [[CrossRef](#)] [[PubMed](#)]
- Heinz, E.; Mettenleiter, M.; Kuhlmann, H.; Holst, C. Strategy for determining the stochastic distance characteristics of the 2d laser scanner Z + F profiler 9012a with special focus on the close range. *Sensors* **2018**, *18*, 2253. [[CrossRef](#)] [[PubMed](#)]
- Alonso, J.M.; Monacelli, B.; Alda, J.; Boreman, G.D. Infrared laser beam temporal fluctuations: Characterization and filtering. *Opt. Eng.* **2005**, *44*, 054203.
- Tamir, M.; Halavee, U.; Azoulay, E. Power fluctuations caused by laser beam wandering and shift. *Appl. Opt.* **1981**, *20*, 734–735. [[CrossRef](#)] [[PubMed](#)]
- Liu, C.S.; Lin, K.W. Numerical and experimental characterization of reducing geometrical fluctuations of laser beam based on rotating optical diffuser. *Opt. Eng.* **2014**, *53*, 122408. [[CrossRef](#)]
- Liu, C.S.; Jiang, S.H. A novel laser displacement sensor with improved robustness toward geometrical fluctuations of the laser beam. *Meas. Sci. Technol.* **2013**, *24*, 105101. [[CrossRef](#)]
- Takeshi, I.; Machida, S.; Nawata, K.; Ikegami, T. Intensity fluctuations in each longitudinal mode of a multimode ALGaAs Laser. *IEEE J. Quantum Electron.* **1977**, *13*, 574–579.
- Skormin, A.; Tascillo, M.A.; Busch, T.E. Adaptive jitter rejection technique applicable to airborne laser communication systems. *Opt. Eng.* **1995**, *34*, 1263–1268.
- Woo, Y.; Kim, C. A controller design for precision laser-beam positioning System. *Int. J. Optomechatron.* **2011**, *5*, 107–127. [[CrossRef](#)]
- Liu, C.-S.; Pu, Y.-F.; Chen, Y.-T.; Luo, Y.-T. Design of a Measurement System for Simultaneously Measuring Six-Degree-Of-Freedom Geometric Errors of a Long Linear Stage. *Sensors* **2018**, *18*, 3875. [[CrossRef](#)] [[PubMed](#)]

12. Matsuo, S.; Yan, L.; Si, J.; Tomita, T.; Hashimoto, S. Reduction of pulse-to-pulse fluctuation in laser pulse energy using the optical Kerr effect. *Opt. Lett.* **2012**, *37*, 1646–1648. [[CrossRef](#)] [[PubMed](#)]
13. Leeuwen, R.V.; Oh, T. Stabilized Laser Using Multiphoton Absorption to Reduce Intensity Fluctuations. U.S. Patent 6,788,715, 9 July 2004.
14. Lu, Y.; Fan, D.; Zhang, Z. Theoretical and experimental determination of bandwidth for a two-axis fast steering mirror. *Optik* **2013**, *124*, 2443–2449. [[CrossRef](#)]
15. Tang, T.; Deng, C.; Yang, T.; Zhong, D.; Ren, G.; Huang, Y.; Fu, C. Error-based observer of a charge couple device tracking loop for fast steering mirror. *Sensors* **2017**, *17*, 479. [[CrossRef](#)] [[PubMed](#)]
16. Deng, C.; Mao, Y.; Ren, G. MEMS inertial sensors-based multi-loop control enhanced by disturbance observation and compensation for fast steering mirror system. *Sensors* **2016**, *16*, 1920. [[CrossRef](#)] [[PubMed](#)]
17. Qingkun, Z.; Ben-Tzvi, P.; Dapeng, F.; Goldenberg, A.A. Design of fast steering mirror systems for precision laser beams steering. In Proceedings of the 2008 International Workshop on Robotic and Sensors Environments, Ottawa, ON, Canada, 17–18 October 2008; pp. 144–149.
18. Lin, P.D. *Advanced Geometrical Optics*; Springer: Singapore, 2017.
19. Greivenkamp, J.E.; Steed, D.L. The history of telescopes and binoculars: An Engineering Perspective. *Proc. SPIE* **2011**, *8129*. [[CrossRef](#)]
20. Zhang, R.; Qu, Y.; Zhao, W. Output-mirror-tuning terahertz-wave parametric oscillator with an asymmetrical porro-prism resonator configuration. *J. Infrared Millim. Terahertz Waves* **2017**, *38*, 653–659. [[CrossRef](#)]
21. Liu, Y.D.; Gao, C.; Qi, X. Field rotation and polarization properties of the Porro prism. *J. Opt. Soc. Am. A* **2009**, *26*, 1157–1160. [[CrossRef](#)]
22. Lin, P.D. Derivatives of optical path length: from mathematical formulation to applications. *J. Opt. Soc. Am. A* **2015**, *32*, 710–717. [[CrossRef](#)] [[PubMed](#)]
23. Chen, Y.T.; Huang, Y.S.; Liu, C.S. An optical sensor for measuring the position and slanting direction of flat surfaces. *Sensors* **2016**, *16*, 1061. [[CrossRef](#)] [[PubMed](#)]
24. Chen, Y.T.; Lin, W.C.; Liu, C.S. Design and experimental verification of novel six degree-of-freedom geometric error measurement system for linear stage. *Opt. Lasers Eng.* **2017**, *92*, 94–104. [[CrossRef](#)]



© 2018 by the authors. Licensee MDPI, Basel, Switzerland. This article is an open access article distributed under the terms and conditions of the Creative Commons Attribution (CC BY) license (<http://creativecommons.org/licenses/by/4.0/>).